Control of motor coordination by astrocytic tonic GABA release through modulation of excitation/inhibition balance in cerebellum

Junsung Woo[a,b], Joo Ok Min[c,d], Dae-Si Kang[c,d], Yoo Sung Kim[c,d], Guk Hwa Jung[e], Hyun Jung Park[f], Sunpil Kim[a,g], Heeyoung An[a,g], Jea Known[a,g], Jeongyeon Kim[a], Insop Shim[f], Hyung-Gun Kim[h], C. Justin Lee[a,b,g,1], and Bo-Eun Yoon[c,d,1]

[a]Center for Neuroscience and Functional Connectomics, Korea Institute of Science and Technology (KIST), 02792 Seoul, Republic of Korea; [b]Neuroscience Program, University of Science and Technology, 34113 Daejeon, Republic of Korea; [c]Department of Molecular Biology, Dankook University, Cheonan, 31116 Chungnam, Republic of Korea; [d]Department of Nanobiomedical Science, Dankook University, Cheonan, 31116 Chungnam, Republic of Korea; [e]College of Pharmacy, Dankook University, Cheonan, 31116 Chungnam, Republic of Korea; [f]Department of Physiology, School of Medicine, Kyung Hee University, 02454 Seoul, Republic of Korea; [g]Korea University (KU)-KIST Graduate School of Converging Science and Technologies, Korea University, 02841 Seoul, Republic of Korea; and [h]Department of Pharmacology, College of Medicine, Dankook University, 31116 Cheonan, Republic of Korea

Edited by Solomon H. Snyder, Johns Hopkins University School of Medicine, Baltimore, MD, and approved April 3, 2018 (received for review December 6, 2017)

Tonic inhibition in the brain is mediated through an activation of extrasynaptic $GABA_A$ receptors by the tonically released GABA, resulting in a persistent GABAergic inhibitory action. It is one of the key regulators for neuronal excitability, exerting a powerful action on excitation/inhibition balance. We have previously reported that astrocytic GABA, synthesized by monoamine oxidase B (MAOB), mediates tonic inhibition via GABA-permeable bestrophin 1 (Best1) channel in the cerebellum. However, the role of astrocytic GABA in regulating neuronal excitability, synaptic transmission, and cerebellar brain function has remained elusive. Here, we report that a reduction of tonic GABA release by genetic removal or pharmacological inhibition of Best1 or MAOB caused an enhanced neuronal excitability in cerebellar granule cells (GCs), synaptic transmission at the parallel fiber-Purkinje cell (PF-PC) synapses, and motor performance on the rotarod test, whereas an augmentation of tonic GABA release by astrocyte-specific overexpression of MAOB resulted in a reduced neuronal excitability, synaptic transmission, and motor performance. The bidirectional modulation of astrocytic GABA by genetic alteration of Best1 or MAOB was confirmed by immunostaining and in vivo microdialysis. These findings indicate that astrocytes are the key player in motor coordination through tonic GABA release by modulating neuronal excitability and could be a good therapeutic target for various movement and psychiatric disorders, which show a disturbed excitation/inhibition balance.

tonic GABA | astrocyte | cerebellum | neuronal excitability | motor coordination

Proper brain function requires a balanced excitation and inhibition in synaptic transmission through regulation of neuronal excitability. Neuronal excitability is regulated by inhibitory synaptic transmission, which occurs primarily through GABAergic signaling. It has been reported that interactions between tonically released GABA and extrasynaptically localized high-affinity $GABA_A$ receptors ($GABA_A$Rs) mediate tonic inhibition, which effectively inhibits neuronal excitability (1–5).

Tonic inhibition has been found in various brain regions, including cerebellum, hippocampus, and thalamus (3, 5, 6). Among these brain regions, the role of tonic inhibition in neuronal excitability, synaptic transmission, and brain function has been intensively studied in the cerebellum (3, 7–9). Tonic inhibition modulates the excitability of cerebellar granule cells (GCs), which have an exclusive expression of extrasynaptic $GABA_A$Rs (10, 11), and subsequently influences synaptic transmission at parallel fiber (PF)-Purkinje cell (PC) synapses (3, 7). However, the relationship between tonic inhibition and motor performance has not been clearly demonstrated.

We have previously reported that cerebellar tonic inhibition is mediated by astrocytic GABA release through bestrophin 1 (Best1) from Bergmann glia and lamellar astrocytes (12). We have further reported that the astrocytic GABA is synthesized by the astrocytic mitochondrial enzyme monoamine oxidase B (MAOB) via the putrescine degradation pathway (13). However, in vivo function of the astrocytic GABA-mediated tonic inhibition has not been elucidated. Here, we investigated the modulation of neuronal excitability, synaptic transmission, and motor performance in the cerebellum by manipulating the level of astrocytic tonic GABA using various genetic and pharmacological tools.

Results

To test whether the genetic deletion of the GABA-releasing channel Best1 leads to an alteration of tonic inhibition, we measured the GABAzine-sensitive tonic current in cerebellar GCs from the acutely prepared cerebellar slices of Best1 knockout (KO) mice and compared with the wild-type (WT) mice as previously described (12, 13) (Fig. 1*A*). GCs, but not PCs, are known to express the high-affinity, nondesensitizing, extrasynaptic $GABA_A$Rs composed of α6, β,

Significance

Tonic inhibition plays critical roles in cognitive functions under physiological and pathological conditions by controlling neuronal excitability. Although we have previously reported that cerebellar tonic inhibition is critically dependent on both the synthesis of GABA through monoamine oxidase B (MAOB) enzyme and the release via the bestrophin 1 (Best1) channel, the role of astrocytic GABA in cerebellar function in vivo has remained elusive. Here, we report that a reduction of tonic GABA release by genetic or pharmacological removal of Best1 or MAOB caused enhanced neuronal excitability, synaptic transmission, and motor performance on the rotarod test, whereas an augmentation of tonic GABA release by astrocyte-specific overexpression of MAOB caused opposite results. Our findings suggest the actions of astrocytic GABA in excitation/inhibition balance and motor coordination.

Author contributions: C.J.L. and B.-E.Y. designed research; J.W., J.O.M., D.-S.K., Y.S.K., H.J.P., S.K., J. Known, and J. Kim performed research; G.H.J., H.A., I.S., and H.-G.K. analyzed data; and J.W. and C.J.L. wrote the paper.

The authors declare no conflict of interest.

This article is a PNAS Direct Submission.

[1]To whom correspondence may be addressed. Email: cjl@kist.re.kr or boeunyoon@dankook.ac.kr.

This article contains supporting information online at www.pnas.org/lookup/suppl/doi:10.1073/pnas.1721187115/-/DCSupplemental.

and δ subunits in the cerebellum (10, 11, 14). The successful deletion of Best1 in Best1 KO mice was confirmed by a significant reduction of Best1 immunoreactivity in GFAP-positive lamellar and Bergmann glial cells (*SI Appendix*, Fig. S1). There was no significant difference in GFAP level between WT and Best1 KO mice (*SI Appendix*, Table S1). Best1 KO mice showed a significant reduction of tonic current by about 70% compared with WT mice in cerebellar GCs (Fig. 1 *B*–*D*). This was consistent with our previous findings based on the astrocyte-specific acute gene-silencing system using a Best1-specific shRNA (12). This reduction of tonic current was not due to changes of extrasynaptic $GABA_AR$ expression in Best1 KO mice, as evidenced by no significant difference in amplitude of the tonic current obtained in the presence of the saturating concentration of GABA at 5 μM (15) (Fig. 1 *E*–*G*) or 0.5 μM THIP [4,5,6,7-tetrahydroisoxazolo(5,4-c)pyridin-3-ol], a specific agonist for a δ-subunit–containing $GABA_AR$ (16, 17) (*SI Appendix*, Fig. S2 *B* and *C*). There was no significant difference between WT and Best1 KO in the amplitude and frequency of spontaneous inhibitory synaptic currents, whose representative decay kinetics showed comparable values to those of previous studies utilizing similarly aged animals (10, 17, 18) (*SI Appendix*, Fig. S2 *D*–*F* and Table S2).

Recently, we reported that unlike the GABAergic neurons utilizing glutamic acid decarboxylase, the astrocytes in the cerebellum, as well as the reactive astrocytes in the diseased hippocampus, synthesize GABA using MAOB (1, 13, 19). To test whether increasing the MAOB expression level in astrocytes affects the degree of tonic inhibition, we utilized the doxycycline-dependent MAOB overexpression mouse system under the astrocyte-specific GFAP promoter (GFAP-MAOB; Fig. 1*H*) (20). Compared with the off-doxycycline condition (–Dox), astrocyte-specific overexpression of MAOB by doxycycline (+Dox) significantly enhanced the tonic current in cerebellar GCs by about 30% (Fig. 1 *I*–*K*). However, there was no difference in the 5-μM GABA-induced tonic current

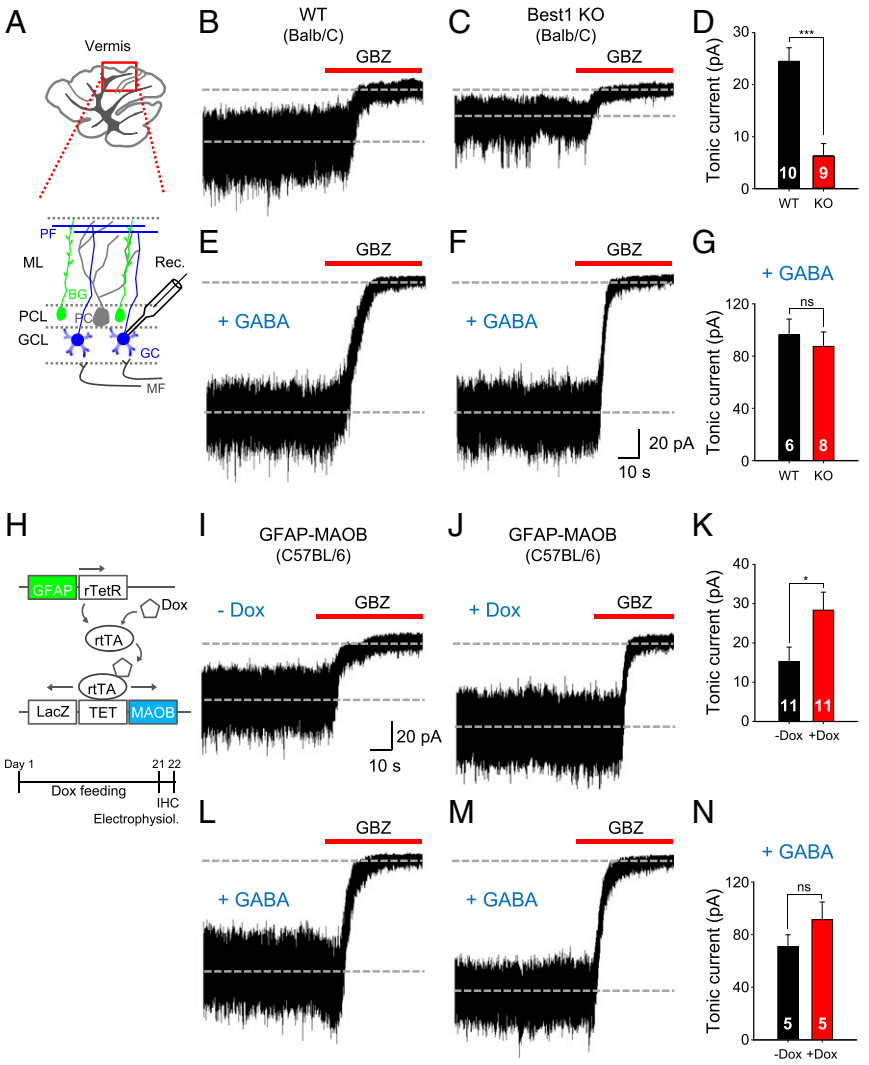

Fig. 1. Suppression of tonic inhibition by genetic deletion of Best1 and enhancement by overexpression of MAOB. (*A*) Schematic illustration for tonic current recording in cerebellar GCs by whole-cell patch clamp. (*B*, *C*, *E*, and *F*) Representative traces of tonic current in cerebellar GCs from WT mice (*B* and *E*) and Best1 KO mice (Balb/C strain) (*C* and *F*). +GABA indicates the adding of 5 μM GABA in the recording solution. (*D* and *G*) The magnitude of 50-μM GABAzine-sensitive tonic current as indicated (unpaired *t* test). (*H*) Schematic showing doxycycline (Dox)-dependent MAOB overexpression in astrocytes. (*I*, *J*, *L*, and *M*) Representative traces of tonic current from GFAP-MAOB mice (C57BL/6 strain) in –Dox (*I* and *L*) and +Dox (*J* and *M*) conditions. +GABA indicates the adding of 5 μM GABA in the recording solution. (*K* and *N*) The magnitude of GABAzine-sensitive tonic current as indicated (unpaired *t* test). Error bars are SEM; $*P < 0.05$; $***P < 0.001$; ns indicates $P > 0.05$. BG, Bergmann glia; GBZ, GABAzine; GCL, GC layer; IHC, immunohistochemistry; MF, mossy fiber; ML, molecular layer; PCL, PC layer; Rec., recording pipette; rtTA, reverse tetracycline responsive transactivator; TET, tetracycline-responsive promoter.

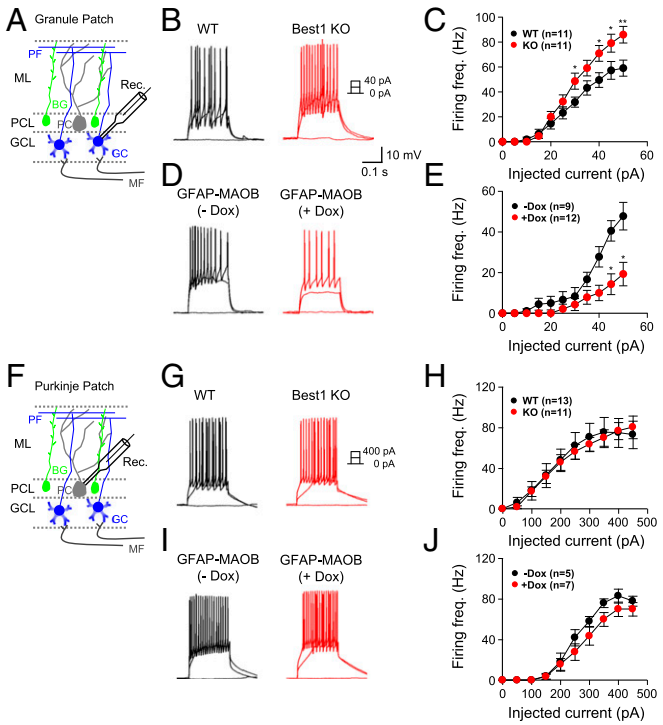

Fig. 2. Modulating tonic inhibition regulates excitability in GCs, but not in PCs. (*A* and *F*) Schematic illustration for measurement of excitability in GCs (*A*) and PCs (*F*) by current injection. BG, Bergmann glia; GCL, GC layer; MF, mossy fiber; ML, molecular layer; PCL, PC layer; Rec., recording pipette. (*B*, *D*, *G*, and *I*) Representative traces of excitatory postsynaptic potentials from WT and Best1 KO mice and GFAP-MAOB mice in −Dox and +Dox conditions. (*C*, *E*, *H*, and *J*) Summary data of firing frequency in GCs and PCs upon varying the injected current (unpaired *t* test). Error bars are SEM; $*P < 0.05$; $**P < 0.01$.

between +Dox and −Dox conditions (Fig. 1 *L*–*N*), indicating no difference in the extrasynaptic $GABA_A$Rs. In addition, there was no significant change in synaptic responses between +Dox and −Dox conditions (*SI Appendix*, Table S2). The increased level of astrocytic GABA in +Dox mice was independently confirmed by immunohistochemistry using a GABA-specific antibody (*SI Appendix*, Fig. S3 *A*–*C*). There was no significant difference in GFAP level between +Dox and −Dox conditions (*SI Appendix*, Table S1). These results strongly support that the astrocytic GABA is synthesized by MAOB, and the cerebellar tonic inhibition is mediated by the tonic release of astrocytic GABA through Best1.

The tonically released astrocytic GABA should exert a strong inhibitory effect on the neighboring neurons, resulting in the change of neuronal excitability and synaptic transmission. To test this possibility, we first measured the intrinsic excitability of GCs and PCs in Best1 KO and GFAP-MAOB mice. We found that the frequency of the current injection-induced action potential firing (Fig. 2*B*) was steadily increased by increasing the amount of injected current (Fig. 2*C*). In Best1 KO mice, we found a significantly higher firing rate compared with WT littermates at high injected currents (Fig. 2*C*). These results are consistent with the previous report that pharmacologically inhibited tonic inhibition increased the excitability of GCs (3). In contrast, we found the opposite results in GFAP-MAOB mice, with a lower firing rate from +Dox condition compared with −Dox condition (Fig. 2 *D* and *E*). Interestingly, the intrinsic excitability of PCs was not different in both types of mice (Fig. 2 *G*–*J*), consistent with the fact that PCs do not have high-affinity, extrasynaptic $GABA_A$Rs. There was no difference in the resting membrane potential of GCs in these mice [WT, −67.8 ± 1.93 mV; Best1 KO, −64.64 ± 2.18 mV ($P = 0.29$) and −Dox, −65 ± 2.32 mV; +Dox, −64 ± 1.91 mV ($P = 0.24$)]. These results demonstrate that the astrocytic GABA exerts a strong inhibitory effect on the intrinsic neuronal excitability of GCs.

Next, we measured the frequency of synaptically induced action-potential firing in PCs—the sole output neuron of the cerebellar cortex and whose activity is controlled by GCs through the PF input (21)—upon electrical stimulation of the mossy fiber (MF) or PF at various stimulation frequencies, as previously described (3) (Fig. 3 *A* and *F*). In Best1 KO mice, we found a significantly higher firing rate over most of the stimulation frequencies compared with WT littermates (Fig. 2*C*). These results are consistent with the previous report that pharmacologically inhibited tonic inhibition increased the excitability of PCs (3). However, we found the opposite results in GFAP-MAOB mice, with a lower firing rate from +Dox condition compared with −Dox condition (Fig. 3*E*). There was no difference in the resting membrane potential of PCs in these mice [WT, −62 ± 1.41 mV; Best1 KO, −61 ± 1.45 mV ($P = 0.47$) and −Dox, −65 ± 2.32 mV; +Dox, −64 ± 1.91 mV ($P = 0.75$)]. We found very similar results with electrical stimulation of the PF (Fig. 3 *G*–*J*). To test if tonic inhibition is the cause of the difference in synaptically induced action-potential firing in PCs, we performed the same experiments in the presence of the $GABA_A$R antagonist GABAzine (Fig. 4 *A* and *F*). We found that GABAzine enhanced PC firing induced by stimulation of MF or PF in WT mice, but not in Best1 KO mice (Fig. 4 *E* and *J*), indicating that tonic GABA causes a strong inhibitory action on PCs at the PF-PC synapse.

In addition to action potential measurement, we also examined the paired-pulse ratio (PPR) in PCs by stimulating the PF. We found a lower PPR in Best1 KO mice (*SI Appendix*, Fig. S4 *B* and *C*), indicating that the presynaptic release probability at the

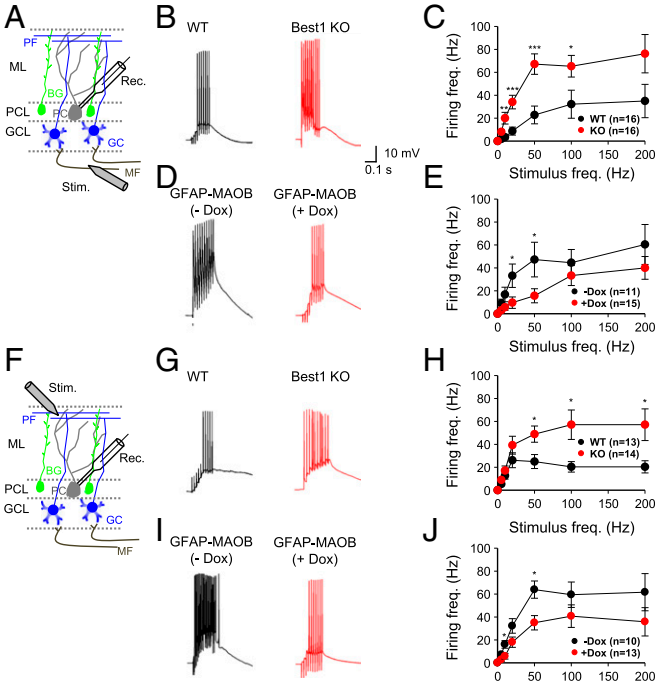

Fig. 3. Modulating tonic inhibition regulates synaptic transmission at MF-PC and PF-PC synapses. (*A* and *F*) Schematic illustration for measurement of excitability in PCs by electrical stimulation (Stim.) of MF (*A*) and PF (*F*). BG, Bergmann glia; GCL, GC layer; ML, molecular layer; PCL, PC layer; Rec., recording pipette. (*B*, *D*, *G*, and *I*) Representative traces of excitatory postsynaptic potentials from WT and Best1 KO mice and GFAP-MAOB mice in −Dox and +Dox conditions (at 50-Hz stimulation). (*C*, *E*, *H*, and *J*) Summary data of firing frequency in PCs at various stimulation frequencies (unpaired *t* test). Error bars are SEM; $*P < 0.05$; $**P < 0.01$; $***P < 0.001$.

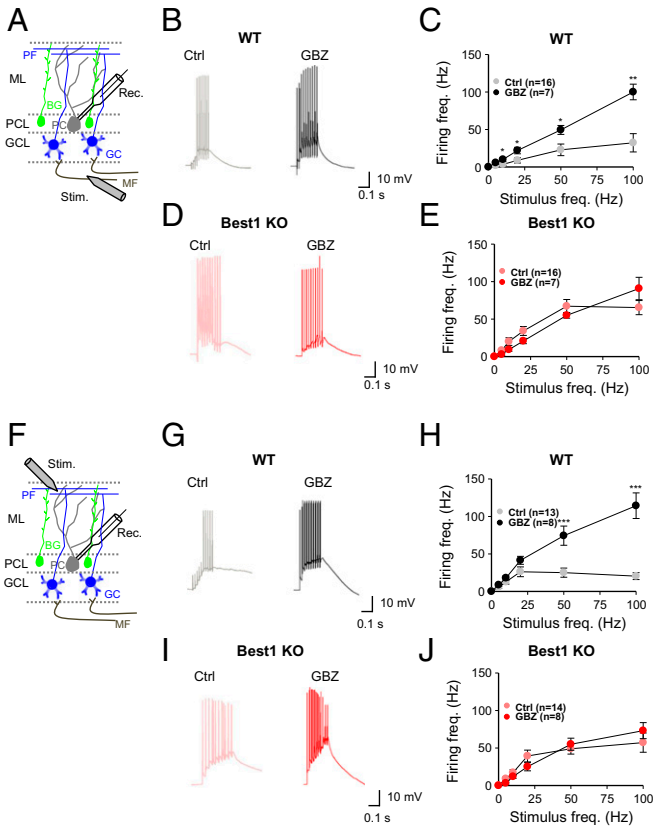

Fig. 4. Astrocytic GABA regulates synaptic transmission at MF-PC and PF-PC synapses. (*A* and *F*) Schematic illustration for measurement of excitability in PCs by electrical stimulation (Stim.) of MF (*A*) and PF (*F*). BG, Bergmann glia; GCL, GC layer; ML, molecular layer; PCL, PC layer; Rec., recording pipette. (*B*, *D*, *G*, and *I*) Representative traces of excitatory postsynaptic potentials from WT and Best1 KO mice with or without treatment of GABAzine (GBZ) (50 μM, at 50-Hz stimulation). Ctrl, control. (*C*, *E*, *H*, and *J*) Summary data of firing frequency in PCs at various stimulation frequencies (unpaired *t* test). Error bars are SEM; $*P < 0.05$; $**P < 0.01$; $***P < 0.001$.

PF-PC synapse in Best1 KO mice was higher than in WT due to a disinhibitory effect in Best1 KO by tonic GABA. We found that first excitatory postsynaptic potential amplitude was significantly enhanced in Best1 KO mice (*SI Appendix*, Fig. S4*D*), indicating that synaptic transmission is enhanced in Best1 KO mice and that tonic GABA is inhibitory at the PF-PC synapse. We measured the synaptic plasticity in terms of long-term potentiation (LTP) at the PF-PC synapse in WT and Best1 KO mice using the widely used stimulation protocol at this synapse (1 Hz, 5 min, 90 stimuli) (22). In WT mice, the LTP was not induced in the absence of inhibitors for GABARs. However, the same stimulation protocol induced a significant LTP in Best1 KO mice (*SI Appendix*, Fig. S4 *F* and *G*). These results support that the astrocytic GABA exerts a strong inhibitory effect on the synaptic transmission, as well as on synaptic plasticity at PF-PC synapses.

To determine the in vivo level of the astrocytic GABA, we directly measured the amount of extracellular GABA using in vivo microdialysis from the cerebellum of freely moving mice (Fig. 5*A*) and the subsequent analysis of the microdialysates by HPLC or mass spectrometry as previously described (1). We found that the extracellular GABA was significantly decreased in both Best1 KO and MAOB KO mice, but slightly increased in +Dox GFAP-MAOB mice compared with WT or −Dox GFAP-MAOB mice (Fig. 5*B*). In contrast, there was no difference in the level of putrescine [the substrate for GABA synthesis (13)], or glutamate (Fig. 5 *C* and *D*).

Lastly, we tested the in vivo function of the astrocytic GABA by performing the rotarod test (Fig. 6*A*), which is a well-known cerebellum-dependent behavior test for motor coordination (23–25). We found that the latency to fall was significantly higher in Best1 KO and MAOB KO mice compared with WT mice (Fig. 6 *C* and *D*). In addition, we utilized selegiline (Fig. 6*B*), which is a selective irreversible MAOB inhibitor and has been previously shown to effectively decrease both the tonic inhibition current in acutely prepared slices and the astrocytic GABA in histological sections (1). We found that the selegiline-treated mice similarly showed a significantly higher latency to fall compared with control mice (Fig. 6*E*). In contrast, +Dox GFAP-MAOB mice showed a significantly lower latency to fall compared with −Dox mice (Fig. 6*F*). These results indicate that the level of astrocytic GABA correlated inversely with the degree of motor coordination. Furthermore, compared with control mice, we found a tendency of increased latency to fall and maximum velocity to stay on the rotarod in both Best1 KO and MAOB KO mice, and a significantly decreased latency to fall and maximum velocity in +Dox GFAP-MAOB mice (*SI Appendix*, Fig. S5), consistent with the inverse correlation between tonic inhibition and motor performance.

Discussion

Here, we have demonstrated that the astrocytic tonic GABA release can control motor coordination by tonically inhibiting cerebellar neuronal excitability (*SI Appendix*, Fig. S6*B*). We found an inverse correlation between the amount of astrocytic GABA and motor performance. Our study raises a possibility of a dynamic control of motor coordination via selective modulation of the release, synthesis, and clearance of astrocytic GABA (*SI Appendix*, Fig. S6*A*).

In the cerebellar circuit, signals enter the cerebellum via MFs, which excite GCs and Golgi cells, which are the sole inhibitory interneuron in the input layer (21). GCs receive inhibitory signals (*i*) from the Golgi cells through the phasic GABA release, with an activation of synaptic $GABA_ARs$ on GCs (3, 11, 26), and (*ii*) from the astrocytes through the tonic GABA release, with an activation of extrasynaptic $GABA_ARs$ containing a δ-subunit on GCs (4, 11–13). GCs have been shown to have exclusive expressions of those extrasynaptic $GABA_ARs$ (10, 11) along their soma, dendrites, and PFs (27). Those extrasynaptic $GABA_ARs$ should be readily activated by GABA released from lamellar astrocytes in the GC layer and Bergmann glial cells along the PFs. In our

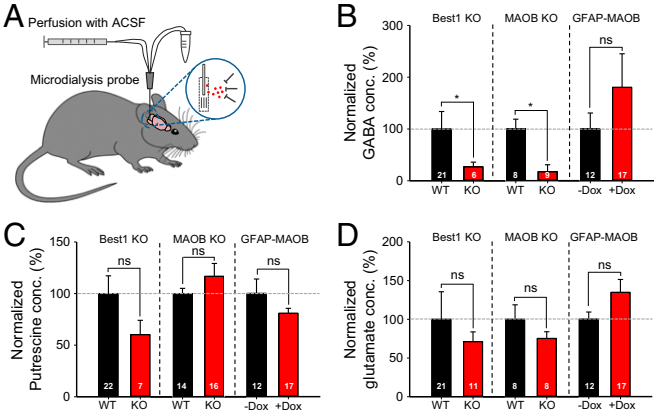

Fig. 5. Extracellular GABA level is decreased by genetic deletion of Best1 or MAOB but increased by overexpression of MAOB. (*A*) Schematic illustration for microdialysis. ACSF, artificial cerebrospinal fluid. (*B–D*) Extracellular GABA (*B*), putrescine (*C*), and glutamate (*D*) concentration from Best1 KO, MAOB KO, and GFAP-MAOB mice (unpaired *t* test). Values were normalized to WT for Best1 KO and MAOB KO.

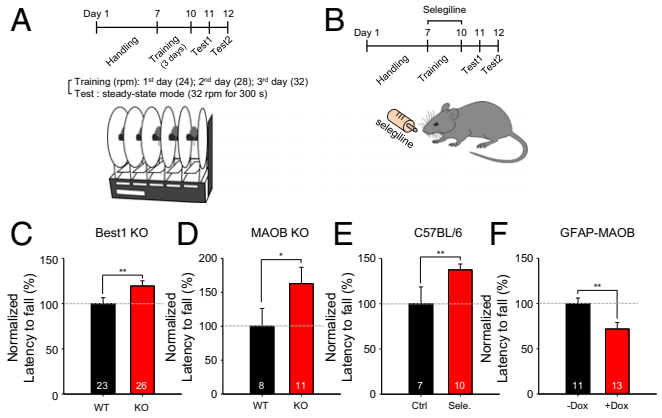

Fig. 6. Motor coordination is enhanced by genetic deletion of Best1 or MAOB but impaired by overexpression of MAOB. (*A*) Experimental timeline and schematic illustration for rotarod test. (*B*) Experimental timeline for selegiline treatment and rotarod test. (*C–F*) Summary graph showing latency to fall during test sessions. Error bars are SEM; $*P < 0.05$; $**P < 0.01$; ns indicates $P > 0.05$. Ctrl, control; Sele., selegiline.

study, we identified a role of astrocytic tonic GABA in the powerful control of GCs' excitability, which synaptically influences the excitability of PCs, the sole source of the cerebellar output. Our results elucidate a mechanism of dynamic regulation of the cerebellar output by controlling the synaptic strength at the PF-PC synapses via tonic inhibition of GCs through the astrocytic tonic GABA release. One can consider the possibility that astrocytic tonic GABA is somehow transiently and locally suppressed, disinhibiting the local GCs in the vicinity and thus allowing particular PF-PC synapses to be activated. This exciting possibility needs future investigations.

We have confirmed that the majority of tonic GABA (70%) is derived from astrocytes through a series of studies using genetic, pharmacological, and molecular tools (12, 13). Nevertheless, there is an unaccounted, remaining portion of tonic GABA current of about 30%. In a very recent study, it has been reported that there is a direct inhibitory signal of PCs to GCs in the forms of both phasic and tonic inhibition modes of action (28). These lines of evidence suggest that PCs can also be a potential source of tonic GABA in GCs. Future studies are needed to test this possibility.

Contrary to our previous and current findings of the Best1-mediated tonic GABA release, Diaz et al. (29) reported that the Best1 channel does not mediate tonic GABAergic current in cerebellar GCs based on only pharmacological evidence using NPPB [5-nitro-2-(3-phenylpropylamino)benzoic acid] as a Best1 channel blocker. However, NPPB is not a specific blocker of Best1 and has many side effects such as inhibiting some potassium and calcium channels (30, 31). Using the cell type-specific gene-silencing method by lentiviral shRNA for Best1 (12) and Best1 KO mice, we unequivocally demonstrate the Best1-mediated tonic GABA release.

We have demonstrated that there was a positive correlation between tonic GABA detected by electrophysiology and extracellular GABA detected by microdialysis, whereas there was no correlation between synaptic GABA and extracellular GABA. These results imply that what we measure in in vivo microdialysis experiments is the level of extracellular tonic GABA rather than synaptically released GABA. Likewise, the extracellular glutamate detected by microdialysis is most likely the level of tonic glutamate, rather than synaptic glutamate, which should be taken up by glutamate transporters in adjacent astrocytes within a couple of seconds (32, 33). It has been reported that ambient glutamate is mediated mostly by the cystine/glutamate antiporter (34). This is probably why we did not detect a significant difference in the level of extracellular glutamate in Best1 KO via in vivo microdialysis. Based on our study, we propose that in vivo microdialysis could be a useful tool to measure the tonic level of extrasynaptic gliotransmitters such as GABA, glutamate, and D-serine.

Although it has been suggested that GCs' excitability and the synaptic transmission between PF and PCs are strongly modulated by tonic inhibition (3, 7, 9), there has been controversy over the effect of GCs' excitability and PF-PC synaptic transmission on cerebellar motor performance. For example, Egawa et al. (9) recently reported that decreased tonic inhibition in GCs resulting in an increase of GCs' excitability caused a dysfunction of motor performance in a mouse model of Angelman syndrome. However, the authors did not measure PF-PC synaptic transmission and tested only the unidirectional manipulation of GCs' excitability. On the other hand, Galliano et al. (8) demonstrated that silencing the majority of PF-PC synaptic transmission through the deletion of P/Q-type Ca^{2+} channels did not affect motor performance. Despite these lines of experimental evidence, the relationship among GCs' excitability, PF-PC synaptic transmission, and motor performance has not been clearly demonstrated. In the current study, we show a clear positive relationship among motor performance, PF-PC synaptic transmission, and GCs' excitability, which are inversely modulated by the astrocytic tonic GABA. We provide multiple lines of evidence from various genetic and pharmacologic mice models through the bidirectional manipulation of GCs' excitability. We clearly demonstrate that less tonic inhibition by genetic removal or pharmacological inhibition of Best1 or MAOB causes an enhanced GC excitability, synaptic transmission in PF-PC synapse, and motor performance, whereas higher tonic inhibition by MAOB overexpression in astrocytes caused a reduced GC excitability, synaptic transmission, and motor performance. Our results are consistent with a previous report demonstrating the inverse correlation between tonic inhibition and sensory-evoked spike output in the cerebellum, although the authors did not show PF-PC synaptic transmission nor motor performance (35).

Many studies have focused on manipulating the extrasynaptic $GABA_AR$, the molecular target for the tonically released GABA, to investigate the functional role of tonic inhibition in the brain (36–38). However, due to a variety of $GABA_AR$ subunits, consisting of 16 subunits and the pentameric composition plus each subunit's differential regional expression pattern (4, 39), it has been extremely difficult to study the in vivo function of the tonic inhibition. Through a series of previous papers, we have demonstrated that the cerebellar tonic inhibition is mediated by the astrocytic GABA, synthesized by astrocyte-specific MAOB enzyme, and released via the GABA-permeable Best1 channel (1, 12, 13). The molecular, genetic, and pharmacological tools that we have characterized in this study should make it possible to selectively manipulate tonic inhibition without disturbing phasic inhibition. These tools will prove useful for studying the role of astrocytic GABA and tonic inhibition in physiological conditions as well as in pathophysiological conditions, including psychiatric disorders such as depression, seizure, stress, schizophrenia, and autism, in which the excitation/inhibition balance has been compromised.

Conclusions

We have reported that the cerebellar tonic inhibition is critically dependent on both MAOB-dependent GABA synthesis and Best1-mediated GABA release. By utilizing this mechanistic insight, we have demonstrated the role of astrocytic GABA in cerebellar motor function by modulating neuronal excitability and synaptic transmission (*SI Appendix*, Fig. S6*B*). We suggest that astrocytes are one of the key components for regulating the cerebellar circuit and output and motor coordination through the tonic release of GABA from astrocytes.

Methods

Animals. Adult (~8 to 10 wk) male and female WT of Best1 KO (Balb/C background), MAOB KO (129 background), and GFAP-MAOB (C57BL/6 background) mice (20) were used. All experimental procedures described below were performed in accordance with Korea Institute of Science and Technology (approval no. 2016-051) and Dankook University (approval no. DKU-17-022) Animal Experimentation Guidelines.

Slice Recording. Cerebellar slicing and slice recording were performed as previously described (12, 13), within a normal artificial cerebrospinal fluid (ACSF) solution that contained 130 mM NaCl, 24 mM $NaHCO_3$, 1.25 mM NaH_2PO_4, 3.5 mM KCl, 1.5 mM $CaCl_2$, 1.5 mM $MgCl_2$, and 10 mM D(+)-glucose, pH 7.4.

Statistical Analysis. The significance of data for comparison was assessed by Student's two-tailed unpaired *t* test. Data are presented as mean ± SEM. Levels of statistical significance are indicated as follows: $*P < 0.05$, $**P < 0.01$, and $***P < 0.001$.

For full, detailed materials and methods, see *SI Appendix, Materials and Methods*.

ACKNOWLEDGMENTS. This study was supported by the Creative Research Initiative Program through the National Research Foundation (NRF) of Korea (Grant 2015R1A3A2066619); the Korea Institute of Science and Technology (KIST) Institutional Grant 2E26662; and the Korea University (KU)-KIST Graduate School of Science and Technology program (Grant R1435281) (to C.J.L.). This research was also supported by the Brain Research Program through the NRF of Korea, funded by the Ministry of Science, ICT, & Future Planning (Grant NRF-2016M3C7A1905074); and the Small Grant for Exploratory Research Program (Grant NRF-2016R1D1A1A02937398) (to B.-E.Y.).

1. Jo S, et al. (2014) GABA from reactive astrocytes impairs memory in mouse models of Alzheimer's disease. *Nat Med* 20:886–896.
2. Semyanov A, Walker MC, Kullmann DM, Silver RA (2004) Tonically active GABA A receptors: Modulating gain and maintaining the tone. *Trends Neurosci* 27:262–269.
3. Hamann M, Rossi DJ, Attwell D (2002) Tonic and spillover inhibition of granule cells control information flow through cerebellar cortex. *Neuron* 33:625–633.
4. Farrant M, Nusser Z (2005) Variations on an inhibitory theme: Phasic and tonic activation of GABA(A) receptors. *Nat Rev Neurosci* 6:215–229.
5. Jia F, et al. (2005) An extrasynaptic GABAA receptor mediates tonic inhibition in thalamic VB neurons. *J Neurophysiol* 94:4491–4501.
6. Lee V, Maguire J (2014) The impact of tonic GABAA receptor-mediated inhibition on neuronal excitability varies across brain region and cell type. *Front Neural Circuits* 8:3.
7. Brickley SG, Cull-Candy SG, Farrant M (1996) Development of a tonic form of synaptic inhibition in rat cerebellar granule cells resulting from persistent activation of GABAA receptors. *J Physiol* 497:753–759.
8. Galliano E, et al. (2013) Silencing the majority of cerebellar granule cells uncovers their essential role in motor learning and consolidation. *Cell Rep* 3:1239–1251.
9. Egawa K, et al. (2012) Decreased tonic inhibition in cerebellar granule cells causes motor dysfunction in a mouse model of Angelman syndrome. *Sci Transl Med* 4: 163ra157.
10. Wall MJ, Usowicz MM (1997) Development of action potential-dependent and independent spontaneous GABAA receptor-mediated currents in granule cells of postnatal rat cerebellum. *Eur J Neurosci* 9:533–548.
11. Nusser Z, Sieghart W, Somogyi P (1998) Segregation of different GABAA receptors to synaptic and extrasynaptic membranes of cerebellar granule cells. *J Neurosci* 18: 1693–1703.
12. Lee S, et al. (2010) Channel-mediated tonic GABA release from glia. *Science* 330: 790–796.
13. Yoon BE, et al. (2014) Glial GABA, synthesized by monoamine oxidase B, mediates tonic inhibition. *J Physiol* 592:4951–4968.
14. Brickley SG, Revilla V, Cull-Candy SG, Wisden W, Farrant M (2001) Adaptive regulation of neuronal excitability by a voltage-independent potassium conductance. *Nature* 409:88–92.
15. Maguire JL, Stell BM, Rafizadeh M, Mody I (2005) Ovarian cycle-linked changes in GABA(A) receptors mediating tonic inhibition alter seizure susceptibility and anxiety. *Nat Neurosci* 8:797–804.
16. Meera P, Wallner M, Otis TS (2011) Molecular basis for the high THIP/gaboxadol sensitivity of extrasynaptic GABA(A) receptors. *J Neurophysiol* 106:2057–2064.
17. Kaplan JS, Mohr C, Rossi DJ (2013) Opposite actions of alcohol on tonic GABA(A) receptor currents mediated by nNOS and PKC activity. *Nat Neurosci* 16:1783–1793.
18. Kaplan JS, et al. (2016) Alcohol suppresses tonic GABAA receptor currents in cerebellar granule cells in the prairie vole: A neural signature of high-alcohol-consuming genotypes. *Alcohol Clin Exp Res* 40:1617–1626.
19. Yarishkin O, Lee J, Jo S, Hwang EM, Lee CJ (2015) Disinhibitory action of astrocytic GABA at the perforant path to dentate gyrus granule neuron synapse reverses to inhibitory in Alzheimer's disease model. *Exp Neurobiol* 24:211–218.
20. Mallajosyula JK, et al. (2008) MAO-B elevation in mouse brain astrocytes results in Parkinson's pathology. *PLoS One* 3:e1616.
21. Shepherd GM (2004) *The Synaptic Organization of the Brain* (Oxford Univ Press, Oxford), 5th Ed.
22. Emi K, et al. (2013) Reevaluation of the role of parallel fiber synapses in delay eyeblink conditioning in mice using Cbln1 as a tool. *Front Neural Circuits* 7:180.
23. Jones BJ, Roberts DJ (1968) The quantiative measurement of motor inco-ordination in naive mice using an acelerating rotarod. *J Pharm Pharmacol* 20:302–304.
24. Caston J, Jones N, Stelz T (1995) Role of preoperative and postoperative sensorimotor training on restoration of the equilibrium behavior in adult mice following cerebellectomy. *Neurobiol Learn Mem* 64:195–202.
25. Lalonde R, Bensoula AN, Filali M (1995) Rotorod sensorimotor learning in cerebellar mutant mice. *Neurosci Res* 22:423–426.
26. Farrant M, Brickley SG (2003) Properties of GABA(A) receptor-mediated transmission at newly formed Golgi-granule cell synapses in the cerebellum. *Neuropharmacology* 44:181–189.
27. Berglund K, Wen L, Dunbar RL, Feng G, Augustine GJ (2016) Optogenetic visualization of presynaptic tonic inhibition of cerebellar parallel fibers. *J Neurosci* 36:5709–5723.
28. Guo C, et al. (2016) Purkinje cells directly inhibit granule cells in specialized regions of the cerebellar cortex. *Neuron* 91:1330–1341.
29. Diaz MR, Wadleigh A, Hughes BA, Woodward JJ, Valenzuela CF (2012) Bestrophin1 channels are insensitive to ethanol and do not mediate tonic GABAergic currents in cerebellar granule cells. *Front Neurosci* 5:148.
30. Fioretti B, et al. (2004) NPPB block of the intermediate-conductance Ca2+-activated K+ channel. *Eur J Pharmacol* 497:1–6.
31. Reinach PS, Schoen HF (1990) NPPB inhibits the basolateral membrane K+ conductance in the isolated bullfrog cornea. *Biochim Biophys Acta* 1026:13–20.
32. Parsons MP, et al. (2016) Real-time imaging of glutamate clearance reveals normal striatal uptake in Huntington disease mouse models. *Nat Commun* 7:11251.
33. Anderson CM, Swanson RA (2000) Astrocyte glutamate transport: Review of properties, regulation, and physiological functions. *Glia* 32:1–14.
34. Augustin H, Grosjean Y, Chen K, Sheng Q, Featherstone DE (2007) Nonvesicular release of glutamate by glial xCT transporters suppresses glutamate receptor clustering in vivo. *J Neurosci* 27:111–123.
35. Duguid I, Branco T, London M, Chadderton P, Häusser M (2012) Tonic inhibition enhances fidelity of sensory information transmission in the cerebellar cortex. *J Neurosci* 32:11132–11143.
36. Brickley SG, Mody I (2012) Extrasynaptic GABA(A) receptors: Their function in the CNS and implications for disease. *Neuron* 73:23–34.
37. Accardi MV, Brown PM, Miraucourt LS, Orser BA, Bowie D (2015) α6-containing GABAA receptors are the principal mediators of inhibitory synapse strengthening by insulin in cerebellar granule cells. *J Neurosci* 35:9676–9688.
38. Engin E, et al. (2013) Alpha5-containing GABAA receptors in dentate gyrus enable cognitive flexibility. *FASEB J* 27(1 Suppl):661.7.
39. Sigel E, Steinmann ME (2012) Structure, function, and modulation of GABA(A) receptors. *J Biol Chem* 287:40224–40231.

Supporting information

Control of motor coordination by astrocytic tonic GABA release through modulation of excitation/inhibition balance in cerebellum

Junsung Woo, Joo Ok Min, Dae-Si Kang, Yoo Sung Kim, Guk Hwa Jung, Hyun Jung Park, Sunpil Kim, Heeyoung An, Jea Kwon, Jeongyeon Kim, Insop Shim, Hyung-Gun Kim, C. Justin Lee† and Bo-Eun Yoon†

†To whom correspondence should be addressed:

C. Justin Lee, Ph.D.
Director of Glia-Neuron Interaction
Korea Institute of Science and Technology (KIST)
5, Hwarang-or 14-gil, Seongbuk-gu
Seoul, 02792, Republic of Korea
Phone: 82-2-958-6940
Fax: 82-2-958-6937
Email: cjl@kist.re.kr

Bo-Eun Yoon, Ph.D.
Department of Molecular biology
Department of Nanobiomedical Science, Dankook University
Dandaero 119, Cheonan, Chungnam 31116, Republic of Korea
Phone: 82-41-550-3694
E-mail: boeunyoon@dankook.ac.kr

This PDF file includes:

Materials and Methods

Animals

Adult (8~10 week) male and female wild-type of Best1 KO (Balb/C background), MAOB KO (129 background) and GFAP-MAOB(1) (C57BL/6 background) mice were used. In GFAP-MAOB mice, astrocyte-specific transgene expression of MAOB was induced by feeding animals with doxycycline at 3000 ppm provided in pre-mixed Purina chow (Research Diets) for a three weeks period. All experimental procedures described below were performed in accordance with KIST (Seoul, Korea, approval number: 2016-051) and Dankook University Animal Experimentation Guidelines (Cheonan, Korea, approval number: DKU-17-022).

Immunohistochemistry

Adult mice were deeply anesthetized with 2% avertin (20 μg/g) and perfused with 0.1M PBS (Phosphate buffered saline) followed by ice cold 4 % PFA (paraformaldehyde). Excised brains were post-fixed overnight in 4 % PFA at 4 °C and immersed in 30% sucrose for 48 hrs for cryo-protection. Parasagittal cerebellar sections (30 μm), rinsed in PBS three times and incubated 1 hr at RT with blocking solution (0.3% Triton-X, 2 % normal serum in 0.1 M PBS). Sections were incubated overnight in a mixture of the following primary antibodies with blocking solution at 4 °C on shaker; rabbit anti bestrophin antibody (1:200; produced by Young In Frontier), rabbit anti MAOB antibody (1:200), chicken anti GFAP antibody (1:500; Millipore) and guinea-pig anti GABA (1:200; Sigma). After washing three times in PBS, sections were incubated with corresponding secondary antibodies; conjugated Alexa 647 goat anti guinea-pig antibody (1:200; Jackson ImmunoResearch Inc.), Alexa 555 goat anti rabbit (1:200; Jackson ImmunoResearch Inc.) and Alexa 488 donkey anti chicken antibody (1:200;

Jackson ImmunoResearch Inc.), for two and a half hours, followed by one rinse in PBS, and incubated one time DAPI (1:1,000) in PBS. After incubated with DAPI, followed by one rinse in PBS. Then mounted with an anti-fade mounting medium. A series of fluorescence images were obtained with a confocal microscope (Zeiss, LSM 700) and images were processed for later analysis using ImageJ program and ZEN 2010 imaging software.

Slice recording

Animals were deeply anesthetized with halothane. After decapitation, the brain was quickly excised from the skull and submerged in an ice-cold cutting solution that contained (in mM): 130 NaCl, 24 $NaHCO_3$, 1.25 NaH_2PO_4, 3.5 KCl, 1.5 $CaCl_2$, 1.5 $MgCl_2$, and 10 D(+)-glucose, pH 7.4. The whole solution was gassed with 95 % O_2-5 % CO_2. After trimming the cerebellar brain, 250 μm parasagittal slices were cut using a vibratome (DSK Linear Slicer, Kyoto, Japan) with a blade (DORCO, Seoul, Korea) and transferred to extracellular ACSF solution (in mM): 130 NaCl, 24 $NaHCO_3$, 1.25 NaH_2PO_4, 3.5 KCl, 1.5 $CaCl_2$, 1.5 $MgCl_2$, and 10 D(+)-glucose, pH 7.4.

Slices were incubated at room temperature for at least one hour prior to recording. Slices were transferred to a recording chamber that was continuously perfused with ASCF solution (flow rate = 2 ml/min). The slice chamber was mounted on the stage of an upright Olympus microscope and viewed with a 60X water immersion objective (NA = 0.90) with infrared differential interference contrast optics. Cellular morphology was visualized by CCD camera and Axon Imaging Workbench software. Whole-cell recordings were made from cerebellar granule cell somata located in lobules 2-5. The holding potential was -60 mV. Pipette resistance was typically 8-10 MΩ for GCs and 4-5 MΩ for PCs. The pipette was filled with an internal solution (in mM): 135 CsCl, 4

NaCl, 0.5 $CaCl_2$, 10 HEPES, 5 EGTA, 2 Mg-ATP, 0.5 Na_2-GTP, 10 QX-314, pH adjusted to 7.2 with CsOH (278-285 mOsmol) for current measurement; 140 K-gluconate, 10 HEPES, 7 NaCl, and 2 MgATP adjusted to pH 7.4 with CsOH for voltage measurement. Electrical signals were digitized and sampled at 50 μs intervals with Digidata 1440A and Multiclamp 700B amplifier (Molecular Devices) using pCLAMP 10.2 software. Data were filtered at 2 kHz.

Evoked responses were obtained by concentric bipolar tungsten stimulating electrodes placed in the white matter to activate mossy fibers or in the molecular layer to activate parallel fibers as previously described (2). Trains of stimuli (200 μA) were 200 ms in duration and delivered only every 30 s to prevent changes in synaptic efficacy (3). To avoid the response change by the position of stimulating electrode, the distance between stimulating electrode and recording electrode was matched. This was monitored by the amplitude of stimulating artifact with the same intensity of stimulation (200 μA). PCs were patched with an internal solution (in mM): 140 K-gluconate, 10 HEPES, 7 NaCl, and 2 MgATP adjusted to pH 7.4 with CsOH and their membrane potential were set at -65 mV. LTP in PCs was measured by evoked EPSC responses in recording solution without the antagonists for $GABA_AR$ and $GABA_BR$ and induced by 1Hz, 5 minutes stimulation (90 stimuli) at paraller fiber in the current clamp mode.

Data analysis and statistical analysis

Off-line analysis was carried out using Clampfit, Minianalysis, SigmaPlot and Excel software. The significance of data for comparison was assessed by Student's two-tailed unpaired t test. Exact *P* values are clearly indicated in the Supplementary Tables. In general, data distribution was assumed to be normal but this was not formally tested.

The data distribution was assumed to be normal. Data are presented as mean ± SEM (standard error of the mean). Levels of statistical significance are indicated as follows:

* ($p < 0.05$), ** ($p < 0.01$), *** ($p < 0.001$).

In vivo microdialysis

Mice were anesthetized with 2 % avertin (20 μg/g) and mounted in a stereotaxic frame. After exposing the skull and drilling a hole, a CMA7 guide cannula (CMA Microdialysis) was inserted in the mid cerebellum (AP: -2.0 mm; ML: 0.0 mm from lambda; DV, -2.0 mm). In addition, anchor screws were located in the skull and fixed with Zinc Polycarboxylate dental cement. After mice recovered from anesthesia, a CMA7 microdialysis probe (membrane diameter 0.24 mm, length 1 mm; stainless-steel shaft diameter 0.38 mm) was implanted through the guide cannula. The probe was connected to a CMA100 microinjection pump (CMA Microdialysis) with polyethylene tubing (PE 50) and FEP tubing (INSTECH). Then the probe was perfused with artificial cerebrospinal fluid (ACSF) (in mM: 149 NaCl, 2.8 KCl, 1.2 $MgCl_2$, 1.2 $CaCl_2$, and 5.4 glucose, pH7.4) into the inlet of the probe at a flow rate of 1.5 μl/min. Perfusates from the outlet of the tubing were automatically collected in plastic vials at 8 °C using CMA 470 refrigerated fraction collector. Dialysates were collected over 20 min intervals for 4 hr and used for measurement glutamate, putrescine and GABA from the second samples. Dialysates were stored at -80 °C and then analyzed using Mass spectrometry and HPLC.

Glutamate and GABA measurement using HPLC

1 mg/ml stock solutions of GABA/glutamate standards were prepared in HPLC-grade

water, aliquoted out and stored at −20 °C. Working solutions (1 µg/ml and 5 µg/ml for glutamate; 100 ng/ml and 500 ng/ml for GABA) were prepared daily by dilutions of those stock solutions, aliquoted out and stored at 4 °C until derivatization and analysis. Briefly, the derivatization was performed by mixing 100 µl in vivo microdialysate or standard solutions, 20 µl of daily prepared methanolic o-phthalaldehyde (5 mg/ml), 75 µl borate buffer (pH 9.9) and 5 µl 3-mercaptopropionic acid. The resulting solution was vortexed and analyzed after 1 min at room temperature. The HPLC system consisted of a Waters chromatograph (Waters) with a 200-µl loop (Rheodyne 7725-I) and a fluorescence detector (FLD-Waters spectrofluorometric detector 2475), coupled to an LC-10 AD pump. The system was equipped with a 3-µm particle size (150 mm × 4.6 mm, ID) C18 analytical column (Hibar-Futigsanle RT) and a prepacked column (RT 250-4 E, Merck). An integrator (Empower 2) was used to analyze the chromatographic data. The mobile phase consisted of 0.05 M sodium acetate, tetrahydrofuran and methanol (50:1:49, v:v:v) adjusted to pH 4.0. The mobile phase was filtered through Millipore 0.45-µm Durapore membrane filters and vacuum degassed before use. Chromatographic analyses were performed at 25 ± 2 °C. Compounds were eluted isocratically over a 9-min runtime at a flow rate of 1 ml/min. The fluorescence detector was set at an excitation wavelength of 337 nm and an emission wavelength of 454 nm, low sensitivity and range GABA/glutamate were identified by their characteristic retention times as determined by standard injections. Sample peak areas were measured through the integrator system and compared with the calibration curve standard in order to quantify the amino acid concentrations.

Glutamate, GABA and putrescine measurement using LC-MS/MS

The LC-MS/MS system consisted of an Agilent 1290 series rapid resolution LC system

and a triple quadrupole linear ion trap mass spectrometer (4000 QTRAP) (AB Sciex, Foster City, CA, USA). Chromatographic separation was achieved using a Luna C8 column (100 mm × 2.0 mm, 3 µm, Phenomenex, Torrance, CA, USA). The mobile phases A and B consisted of 0.1% formic acid in water (LC-MS grade) and acetonitrile (LC-MS grade), respectively. The isocratic elution profile was chosen to assay microdialysis samples: 5% B for GABA and glutamate, 75% B for putrescine. The flow rate was run at 0.3 mL/min and the injection volume was 10 µL. The mass spectrometer was optimized for multiple reaction monitoring (MRM) mode using electrospray ionization (ESI) in positive mode. The ion spray voltage was set at 5000 V and the source temperature at 500°C. The m/z transitions were set as 104.0 → 87.0 for GABA, 148.0 → 84.0 for glutamate and 89.0 → 72.0 for putrescine. Data were acquired and analyzed using the software Analyst® version 1.6 (AB Sciex, Foster City, CA, USA).

Rotarod test

The rotarod test was based on a rod with forced motor activity. Mice were handled for 7 days and were trained to walk on the five station rotarod (MED Associates Inc., USA) for 3 days and then tested for 2 days. The rotarod consists of a cylinder with a diameter 5.5 cm on 5 animals can run simultaneously, separated by panels. The test processed constant 32 rpm during 300 seconds for 2 days. Values for latency to fall were averaged results for 2 days. Mice were placed on the stationary rod and recorded time of latency to fall. Interval time of each trial is 10 mins. In accelerating mode, mice were placed on a rotarod that accelerated from 4 to 40 rpm in 5 mins. Mice were trained for 4 sessions (60 seconds per 1 session) in a day at gradually increasing speed day by day (day 1: 24 rpm; day 2: 28 rpm; day 3: 32 rpm) with 60 seconds for 3 days. The

protocol was based on the previous study (4) with our modification as described above. During training sessions, we allowed each animal to have up to three trials to perform additional rotarod test if a mouse falls within 10 seconds. We excluded any mouse that failed to satisfy this criterion. The tests were done for 2 days. In the test session, each trial ended when mice fell off the rod or when the mice ran for 600 seconds. The time when mice dropped form the rod was recorded. The maximal velocity is the rpm was calculated by recorded time. The equation is (40-4)rpm/300sec * (recorded seconds) + 4 rpm.

Supplementary Figures

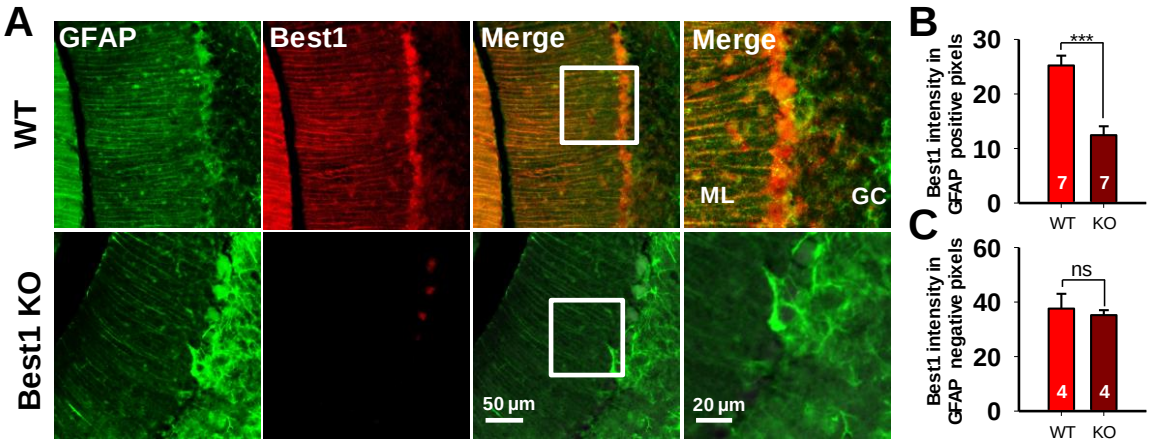

Fig. S1. Confirmation of genetic deletion of Best1 in Best1 KO mice by immunohistochemistry.
(A) Immunostaining from cerebellar slices with wild type and Best1 KO mice. (Green: GFAP; Red: Best1, ML: molecular layer, GC: granule cell layer). **(B and C)** Quantification of Best1 immunoreactivity in GFAP positive pixels (B, WT: 25.21 ± 1.82; KO: 12.91 ± 1.67; *P* = 0.0003) and negative pixels (C, WT: 37.58 ± 5.41; KO: 35.19 ± 1.81; *P* = 0.6904, unpaired t test).

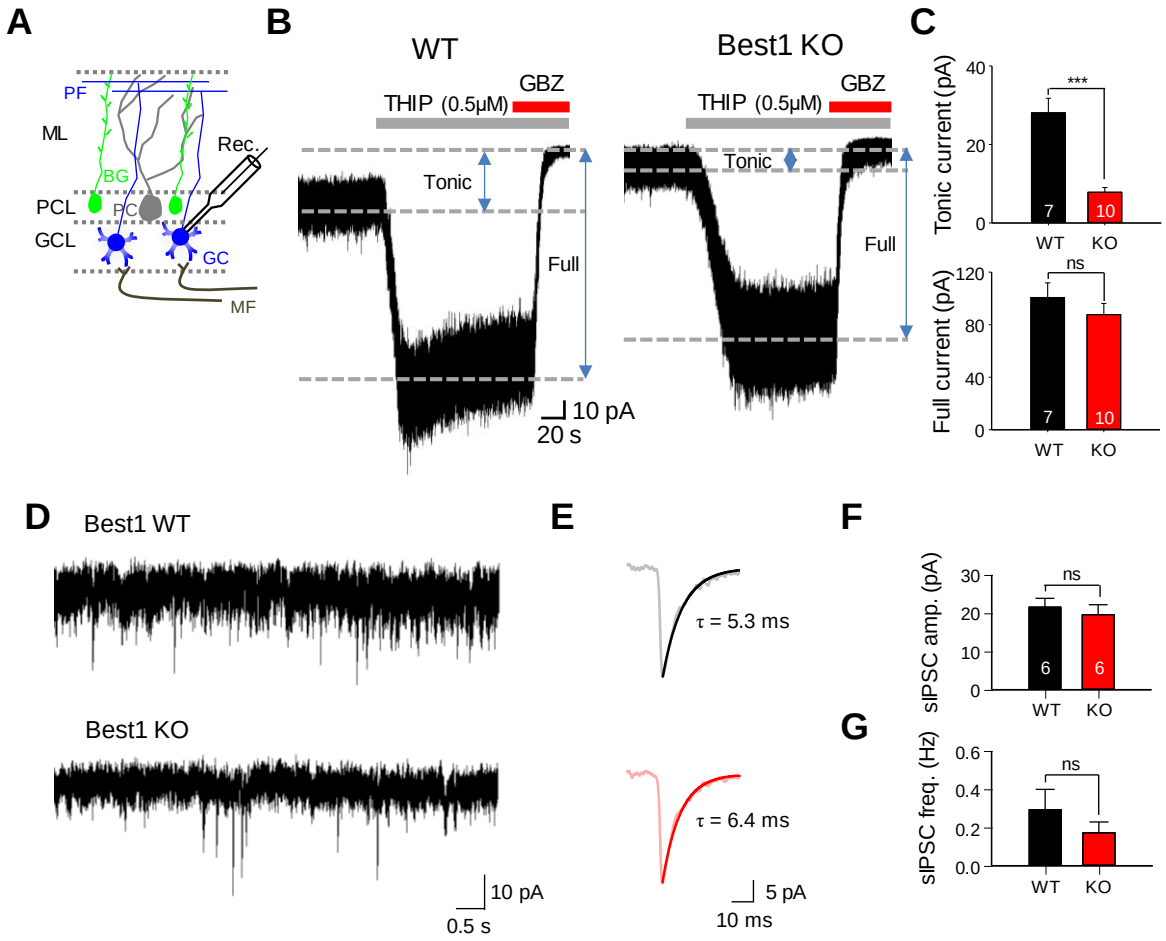

Fig. S2. No significant difference in THIP-induced tonic current and synaptic responses in WT and Best1 KO mice.

(A) Schematic illustration for tonic current recording in cerebellar GCs by whole-cell patch clamp. **(B)** Representative traces of tonic current in cerebellar GCs from WT and Best1 KO mice. **(C)** Magnitude of GABAzine sensitive tonic current (upper, WT: 27.06 ± 2.77 pA; KO: 7.84 ± 1.19 pA; *P* = 0.00003) and full current (bottom, WT: 97.51 ± 8.52; KO: 87.70 ± 8.53 pA; *P* = 0.4248) as indicated (unpaired t test). **(D)** Representative traces of sIPSC from WT and Best1 KO mice. **(E)** Averaged sIPSCs after normalization by peak. Decay was fitted to one-expenential functions. **(F,G)** Summary data of amplitude (F, WT: 21.59 ± 2.28; KO: 19.59 ± 2.59 pA; *P* = 0.5573) and frequency (G, WT: 0.29 ± 0.11; KO: 0.17 ± 0.06 pA; *P* = 0.3043) of sIPSCs. (unpaired t test).

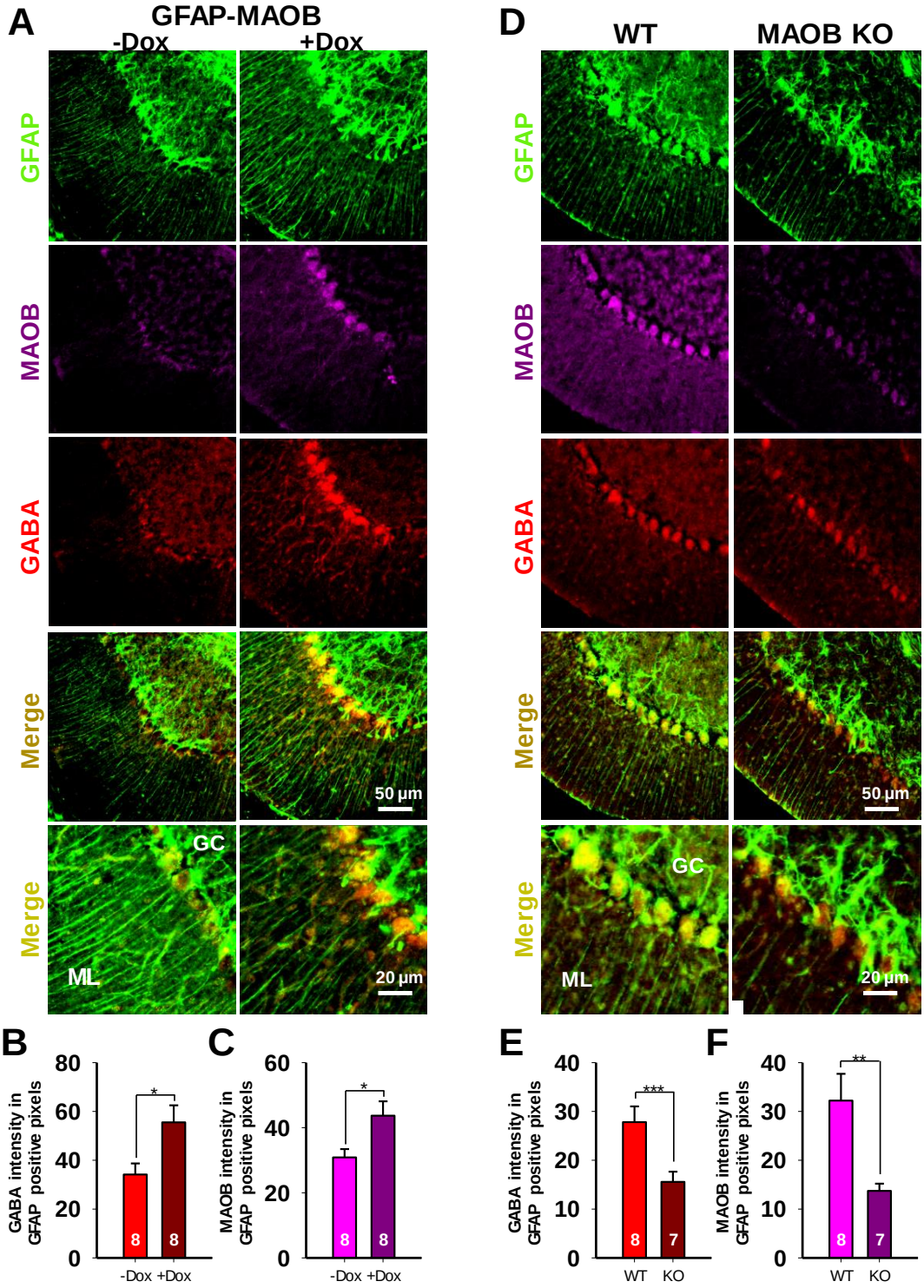

Fig. S3. GABA content is suppressed by genetic deletion of MAOB and enhanced by overexpression of MAOB in Bergmann glial cells and lamellar astrocytes.

(A) Immunostaining from cerebellar slices from GFAP-MAOB mice in off-doxycycline (- Dox) and on-doxycycline (+ Dox) conditions. (Green: GFAP; Purple: MAOB, Red: GABA). **(B and C)** Quantification of GABA (b, - Dox: 34.16 ± 4.82; + Dox: 55.53 ± 7.43, GFAP (+); *P* = 0.022) and MAOB (c, - Dox: 30.87 ± 2.75; + Dox: 43.71 ± 4.72; *P* =

0.025, unpaired t test) immunoreactivity in GFAP positive pixels. **(D)** Immunostaining from cerebellar slices from wild type and MAOB KO mice. (Green: GFAP; Purple: MAOB, Red: GABA). **(E and F)** Quantification of GABA (e, WT: 27.82 ± 3.42; KO: 15.57 ± 2.09; *P* = 0.0084) and MAOB (f, WT: 32.22 ± 5.86; KO: 13.72 ± 1.49; *P* = 0.0009; unpaired t test) immunoreactivity in GFAP positive pixels.

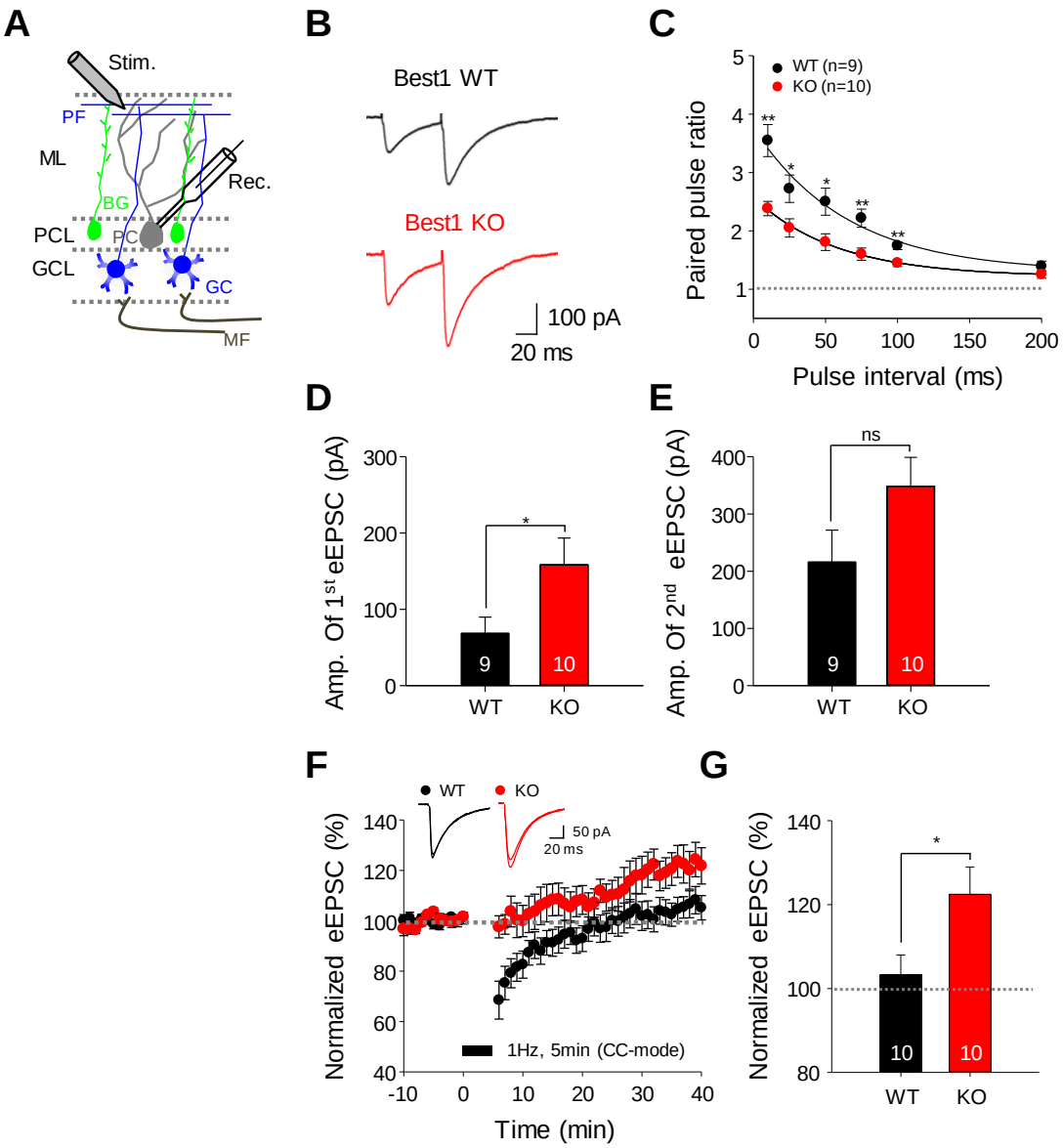

Fig. S4. Release probability and synaptic plasticity are increased in Best1 KO mice.

(A) Schematic illustration for evoked EPSC (eEPSC) in cerebellar PCs by electrical stimulation of PF. **(B)** Representative traces of PPR in PCs from WT and Best1 KO mice. **(C)** Suammary data of PPR in PCs upon various pulse interval (unpaired t test). **(D, E)** Averaged amplitude of eEPSCs in 1st (WT: 68.7 ± 21.16; KO: 158.39 ± 35.09 pA; *P* = 0.046) and 2nd (WT: 99.69 ± 30.41; KO: 178.14 ± 39.46 pA; *P* = 0.014) responses at 10 ms stimulation interval. **(F)** Averaged eEPSC upon LTP protrocol (1Hz, 5 min in current-clamp mode) from WT and Best1 KO mice. **(G)** Summary data of LTP (averaging responses for the last 5 min, WT: 103.29 ± 4.69; KO: 122.46 ± 6.53 %; *P* = 0.0283, unpaired t test).

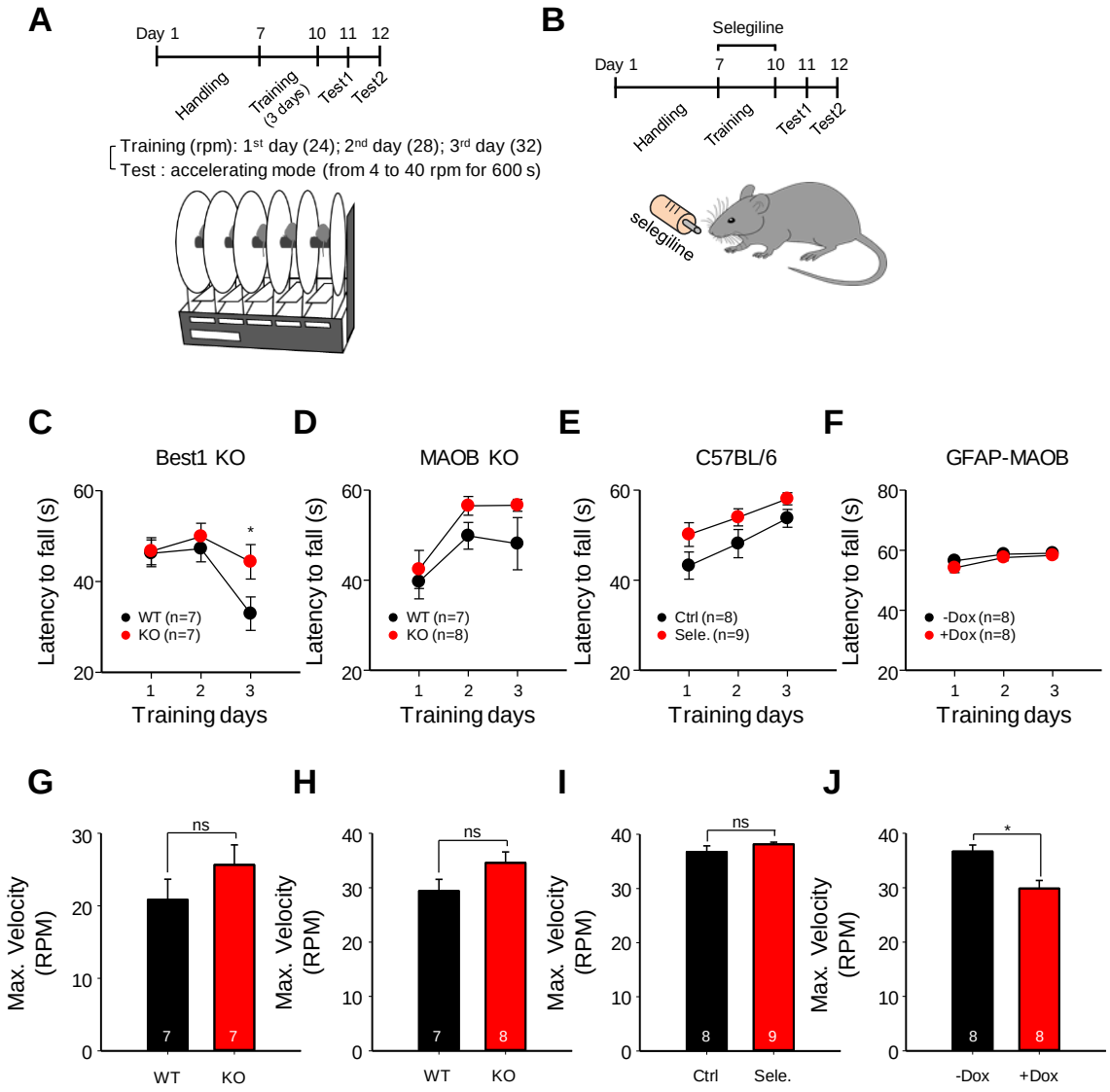

Fig. S5. Initial motor performance and maximum velocity to stay on from rotarod test.

(A) Experimental timeline and schematic illustration for rotarod test. **(B)** Experimental timeline for selegiline treatment and rotarod test. **(C-F)** Summary graph showing latency to fall during training sessions. **(G-J)** Summary graph maximum velocity (unpaired t test). Error bars are s.e.m., * indicates $P < 0.05$, ns indicates $P > 0.05$.

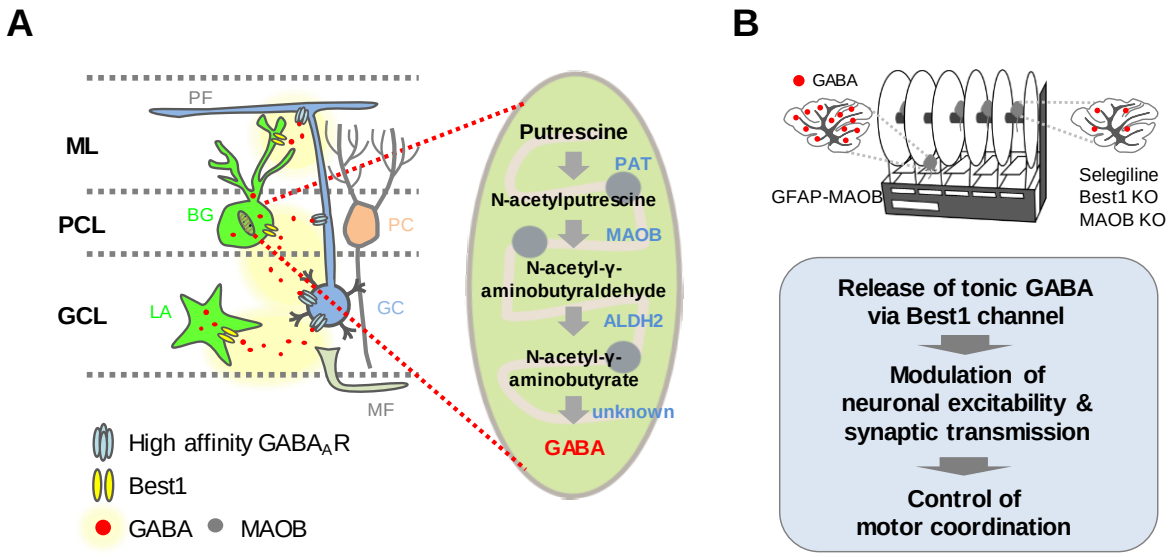

Fig. S6. Schematic model for astrocytic GABA-mediated control of motor coordination.
(A) Schematic for GABA synthesis pathway in cerebellum. PAT: putrescine acetyltransferase; MAOB: monoamine oxidase B; ALDH2: aldehyde dehydrogenase 2. **(B)** Schematic model showing modulation of glial GABA, neuronal excitability, synaptic transmission, and motor coordination.

Supplementary Table 1

	GFAP intensity (a.u.)			
	Avg	SEM	n (slices)	*P* value
Best1 WT	57.02	3.6	7	0.78
Best1 KO	57.15	5.89	7	
MAOB WT	69.07	7.08	8	0.15
MAOB KO	54.69	5.99	7	
GFAP-MAOB (-Dox)	102.55	4.95	8	0.09
GFAP-MAOB (+Dox)	119.47	8.02	8	

Quantification of GFAP intentisity in Best1 KO, MAOB KO, and GFAP-MAOB mice (related to supplementary figure 2). *P*-values were derived from two-tailed unpaired t tests (Avg: mean; SEM: standard error of the mean).

Supplementary Table 2

	sIPSC amplitude (pA)				sIPSC frequency (Hz)			
	Avg	SEM	n (slices)	*P* value	Avg	SEM	n (slices)	*P* value
Best1 WT	15.29	2.05	6	0.58	0.34	0.07	6	0.16
Best1 KO	13.48	2.33	7		0.25	0.02	7	
GFAP-MAOB (-Dox)	16.05	2.09	12	0.16	0.28	0.03	12	0.68
GFAP-MAOB (+Dox)	21.48	3.16	10		0.24	0.09	10	

Results of the amplitude and frequency spontaneous IPSC (sIPSC) from Best1 wildtype, KO mice and GFAP-MAOB (-Dox / +Dox) mice. *P*-values were derived from two-tailed unpaired t tests (Avg: mean; SEM: standard error of the mean).

Supplementary Table 3

Tonic current (pA)					
	Avg	SEM	n (slices)	N (mice)	*P* value
Best1 WT	21.17	1.62	6	3	0.0005
Best1 KO	6.28	2.38	9	3	
Tonic current (pA) in the presence of 5 µM					
	Avg	SEM	n (slices)	N (mice)	*P* value
Best1 WT	93.23	12.07	6	3	0.6023
Best1 KO	87.4	11.05	8	3	

Tonic current (pA)					
	Avg	SEM	n (slices)	N (mice)	*P* value
GFAP-MAOB (-Dox)	15.25	3.97	11	4	0.0384
GFAP-MAOB (+Dox)	28.34	4.88	11	4	
Tonic current (pA) in the presence of 5 µM					
	Avg	SEM	n (slices)	N (mice)	*P* value
GFAP-MAOB (-Dox)	70.94	8.91	5	3	0.2411
GFAP-MAOB (+Dox)	91.34	13.43	5	3	

Results of the tonic current (illustrated in **Fig. 1D,G,K,N**) without or with 5 µM GABA in recording ACSF from Best1 wildtype, KO mice (upper) and GFAP-MAOB (-Dox / +Dox) mice (bottom). *P*values were derived from two-tailed unpaired t tests (Avg: mean; SEM: standard error of the mean).

Supplementary Table 4

EPSP (mV) in GCs by current injection					
	Best1 WT (n=11; N=3)		Best1 KO (n=11; N=3)		
Current (pA)	Avg	SEM	Avg	SEM	*P* value
0	0.00	0.00	0.00	0.00	N/D
5	0.00	0.00	0.00	0.00	N/D
10	1.82	1.82	0.00	0.00	0.3293
15	6.36	3.64	4.55	1.84	0.6603
20	14.55	4.29	20.00	4.32	0.3807
25	23.18	4.83	32.27	5.37	0.2224
30	31.82	4.06	48.64	6.43	0.0389
35	43.18	5.73	59.09	6.25	0.0752
40	49.55	5.90	70.91	6.32	0.0225
45	57.27	7.15	79.09	7.19	0.0438
50	59.09	6.43	85.91	6.67	0.0089
	GFAP-MAOB (-Dox) (n=9; N=3)		GFAP-MAOB (+Dox) (n=12; N=3)		
Current (pA)	Avg	s.e.m.	Avg	s.e.m.	*P* value
0	0.00	0.00	0.00	0.00	N/D
5	0.00	0.00	0.00	0.00	N/D
10	1.11	1.11	0.00	0.00	0.2384
15	4.44	2.94	0.00	0.00	0.0810
20	5.00	3.33	0.00	0.52	0.1484
25	6.67	4.00	2.14	2.32	0.5798
30	8.33	4.33	4.29	2.95	0.6704
35	16.67	3.54	7.86	3.42	0.2288
40	27.78	5.01	10.00	3.80	0.0517
45	40.56	5.03	14.29	5.11	0.0293
50	47.78	6.78	19.29	5.76	0.0360

EPSP (mV) in PCs by current injection					
	Best1 WT (n=13; N=3)		Best1 KO (n=11; N=3)		
Current (pA)	Avg	SEM	Avg	SEM	*P* value
0	0.00	0.00	0.00	0.00	N/D
50	6.15	5.38	1.82	1.39	0.4776
100	18.08	9.14	17.27	4.74	0.9417
150	33.08	11.80	31.82	6.51	0.9301
200	48.08	11.06	45.91	7.74	0.8783
250	62.31	13.10	56.36	7.30	0.7100
300	70.77	13.61	63.64	6.98	0.6633
350	75.38	14.79	70.00	8.06	0.7644
400	75.00	14.18	76.82	8.35	0.9170
450	73.08	13.46	80.45	11.09	0.6835

	GFAP-MAOB (-Dox) (n=5; N=3)		GFAP-MAOB (+Dox) (n=7; N=3)		
Current (pA)	Avg	s.e.m.	Avg	s.e.m.	*P* value
0	0.00	0.00	0.00	0.00	N/D
50	0.00	0.00	0.00	0.00	N/D
100	0.00	0.00	0.00	0.00	N/D
150	4.00	2.92	3.57	2.37	0.9108
200	18.00	8.89	15.71	5.82	0.8263
250	42.00	8.00	27.86	8.15	0.2590
300	58.00	4.90	43.57	8.84	0.2329
350	76.00	4.30	60.00	6.81	0.1031
400	83.00	6.82	70.00	7.07	0.2310
450	78.00	4.90	70.00	6.64	0.3918

Results of the EPSP of GCs by current injection from Best1 WT, KO mice and GFAP-MAOB (-Dox), GFAP-MAOB (+Dox) mice (illustrated in **Fig. 2C, E**, top). Results of the EPSP of PCs by current injection from Best1 WT, KO mice and GFAP-MAOB (-Dox), GFAP-MAOB (+Dox) mice (illustrated in **Fig. 2H, J**, bottom). *P*-values were derived from two-tailed unpaired t tests (Avg: mean; SEM: standard error of the mean; N/D: no detected).

Supplementary Table 5

Evoked EPSP (mV) by MF stimulation					
	Best1 WT (n=16; N=4)		Best1 KO (n=16; N=4)		
Stim. (Hz)	Avg	SEM	Avg	SEM	*P* value
5	1.88	0.9	8.13	1.7	0.0029
10	3.44	1.63	20	5.12	0.0044
20	8.75	3.49	34.06	5.92	0.0009
50	22.81	7.46	67.19	8.93	0.0008
100	32.19	12.24	65.31	9.45	0.0404
200	35	14.54	76.25	16.74	0.0726
Evoked EPSP (mV) by PF stimulation					
	Best1 WT (n=13; N=4)		Best1 KO (n=14; N=4)		
Stim. (Hz)	Avg	s.e.m.	Avg	s.e.m.	*P* value
5	5.38	1.44	8.93	2.23	0.2019
10	12.69	3.03	17.14	4.01	0.3903
20	26.16	6.48	39.29	7.81	0.2112
50	26	6.1	48.93	7.09	0.0177
100	20.38	4.58	57.14	12.84	0.0149
200	20.38	5.32	5.14	13.81	0.0235

Evoked EPSP (mV) by MF stimulation					
	GFAP-MAOB (-Dox) (n=11; N=4)		GFAP-MAOB (+Dox) (n=15; N=4)		
Stim. (Hz)	Avg	SEM	Avg	SEM	*P* value
5	9.09	3.62	3	1.45	0.0959
10	16.82	6.37	5.67	2.62	0.0860
20	33.18	10.21	9.67	4.98	0.0341
50	47.27	15.13	15.67	6.13	0.0423
100	44.55	11.55	33.33	8.72	0.4371
200	60.45	17.44	40	9.93	0.2889
Evoked EPSP (mV) by PF stimulation					
	GFAP-MAOB (-Dox) (n=10; N=4)		GFAP-MAOB (+Dox) (n=13; N=4)		
Stim. (Hz)	Avg	s.e.m.	Avg	s.e.m.	*P* value
5	6.5	1.5	2.69	1.34	0.0731
10	14.5	3.37	5.77	2.46	0.0437
20	29	6.53	18.08	4.48	0.1686
50	57.5	9.29	35	6.23	0.0493
100	53.5	11.55	40.77	9.82	0.4085
200	53.5	15.77	35.83	12.35	0.3310

Results of the evoked EPSP by mossy fiber and parallel fiber stimulation from Best1 wildtype and KO mice (illustrated in **Fig. 3C, H**, top) and GFAP-MAOB (-Dox) and

GFAP-MAOB (+Dox) mice (illustrated in **Fig. 3E, J,** bottom). *P*-values were derived from two-tailed unpaired t tests (Avg: mean; SEM: standard error of the mean).

Supplementary Table 6

Evoked EPSP (mV) by MF stimulation from Best1 WT					
	Control (n=16; N=4)		GABAzine (n=7; N=2)		
Stim. (Hz)	Avg	SEM	Avg	SEM	*P* value
5	2.00	0.95	5.63	1.99	0.0589
10	3.67	1.72	10.00	2.50	0.0338
20	9.33	3.68	21.88	4.32	0.0344
50	24.33	8.12	49.38	5.93	0.0349
100	34.33	12.88	100.00	10.39	0.0017
Evoked EPSP (mV) by MF stimulation from Best1 KO					
	Control (n=16; N=4)		GABAzine (n=7; N=2)		
Stim. (Hz)	Avg	s.e.m.	Avg	s.e.m.	*P* value
5	7.33	1.61	2.86	1.49	0.0983
10	19.00	5.37	9.29	2.30	0.2451
20	32.00	5.93	20.71	3.52	0.2295
50	65.67	9.41	55.00	3.78	0.4607
100	65.33	10.10	90.71	14.94	0.1730

Evoked EPSP (mV) by PF stimulation from Best1 WT					
	Control (n=13; N=4)		GABAzine (n=8; N=2)		
Stim. (Hz)	Avg	SEM	Avg	SEM	*P* value
5	5.38	1.44	8.57	1.43	0.1709
10	12.69	3.03	17.86	2.86	0.2817
20	26.15	6.48	41.43	5.31	0.1336
50	25.00	6.10	74.29	12.79	0.0009
100	20.38	4.58	114.29	17.06	0.0000
Evoked EPSP (mV) by PF stimulation from Best1 KO					
	Control (n=14; N=4)		GABAzine (n=8; N=2)		
Stim. (Hz)	Avg	s.e.m.	Avg	s.e.m.	*P* value
5	8.93	2.23	3.13	1.32	0.0797
10	17.14	4.02	11.88	2.49	0.3646
20	39.29	7.81	25.00	5.43	0.2162
50	48.93	7.09	55.00	8.07	0.5943
100	57.14	12.84	73.13	10.69	0.4078

Results of the evoked EPSP by mossy fiber and parallel fiber stimulation from Best1 wildtype and KO mice (illustrated in **Fig. 4C, E**, bottom) and GFAP-MAOB (-Dox) and GFAP-MAOB (+Dox) mice (illustrated in **Fig. 4H, J**). *P*-values were derived from two-tailed unpaired t tests (Avg: mean; SEM: standard error of the mean).

Supplementary Table 7

Extracellular concertation by microdialysis (%, after normalization)												
	GABA				Glutamate				Putrescine			
	Avg	SEM	N (mice)	*P* value	Avg	SEM	N	*P*	Avg	SEM	N	*P*
Best1 WT	100	18.78	21	0.0183	100	18.73	21	0.3174	100	17.22	22	0.1713
Best1 KO	17.23	13.59	6		75.32	8.68	11		60.26	13.86	7	
MAOB WT	100	33.85	8	0.0441	100	35.56	8	0.4362	100	5.11	14	0.2500
MAOB KO	27.03	9.04	9		71.21	12.59	8		116.69	12.50	16	
GFAP-MAOB (-Dox)	100	30.71	12	0.3339	100	9.18	12	0.0599	100	13.99	12	0.1512
GFAP-MAOB (+Dox)	180.35	64.79	17		134.55	16.69	17		80.75	4.86	17	

Results of the extracellular concentration of GABA, Glutamate, and Putrescine measured by microdialysis (illustrated in **Fig. 5B to D**). *P*-values were derived from two-tailed unpaired t tests (Avg: mean; SEM: standard error of the mean).

Supplementary Table 8

Latency to fall in rotarod test (%, after normalization)				
	Avg	SEM	N (mice)	*P* value
Best1 WT	100	6.62	23	0.0176
Best1 KO	119.51	5.73	26	
MAOB WT	100	26.27	8	0.0989
MAOB KO	162.82	23.99	11	
Control	100	18.65	9	0.0453
Selegiline	137.54	6.37	10	
GFAP-MAOB (-Dox)	100	6.2	8	0.081
GFAP-MAOB (+Dox)	71.97	7.12	11	

Results of the rotarod test (illustrated in **Fig. 6C to F**). *P*-values were derived from two-tailed unpaired t tests (Avg: mean; SEM: standard error of the mean).

References

1. Mallajosyula JK*, et al.* (2008) MAO-B elevation in mouse brain astrocytes results in Parkinson's pathology. *PLoS One* 3(2):e1616.
2. Hamann M, Rossi DJ, & Attwell D (2002) Tonic and spillover inhibition of granule cells control information flow through cerebellar cortex. *Neuron* 33(4):625-633.
3. D'Angelo E, De Filippi G, Rossi P, & Taglietti V (1995) Synaptic excitation of individual rat cerebellar granule cells in situ: evidence for the role of NMDA receptors. *J Physiol* 484 (Pt 2):397-413.
4. Carter RJ, Morton J, & Dunnett SB (2001) Motor coordination and balance in rodents. *Curr Protoc Neurosci* Chapter 8:Unit 8 12.